Computational Geosciences 1 (1997) 251–270 

# A numerical study of fronts in random media using a reactive solute transport model

Marie Postel [a] and Jack Xin [b]

[a] *Laboratoire d'Analyse Numérique, CNRS et Université Pierre et Marie Curie, F-75252 Paris Cedex 05, France*
[b] *Department of Mathematics, University of Arizona, Tucson, AZ 85721, USA*

Received 3 June 1996; revised 24 July 1997

We simulate the random front solutions of a nonlinear solute transport equation with spatial random coefficients modeling inhomogeneous sorption sites in porous media. The nonlinear sorption function is chosen to be Langmuir type, and the random coefficients are two independent stationary processes with fast decay of correlations. The model equation is in conservation form, and the random fronts are similar to random viscous shocks. We find that the average front speed is given by an ensemble averaged explicit Rankine–Hugoniot relation, and the front position fluctuates about its mean. Our numerical calculations show that the standard deviation is of the order O($\sqrt{t}$) for large time, and the front fluctuation scaled by $\sqrt{t}$ converges to a Gaussian random variable wih mean zero. We come up with a formal theory of front fluctuation, yielding an explicit expression of the root $t$ normalized front standard deviation in terms of the random media statistics. The theory agrees remarkably with the numerically discovered empirical formula.

**Keywords:** fronts, random media, solute transport, Gaussian statistics

## 1. Introduction

Contamination of ground-water in industrial and agricultural areas is often associated with large concentrations of heavy metals or organic substance entering soils by means of waste disposal or atmospheric deposition (see [2], etc.). The movement of contaminants involves both physical and chemical processes in the normally complex geological media. To better understand and predict the dynamics of contaminants, mathematical models are of tremendous value in estimating various transport effects and their interactions. In [2,10], the authors studied the following model for transport of reacting solute in one-dimensional heterogeneous porous media subject to nonlinear equilibrium sorption. After a rescaling of constants, the model reads:

$$\big(u + k(x)f(u)\big)_t = \big(D(x)u_x\big)_x - vu_x, \tag{1.1}$$

where $u$ is the solute concentration, $f(u)$ is a nonlinear sorption function, $v$ is a constant water velocity; $D(x)$, the hydraulic dispersion, and $k(x)$, the sorption spatial

variability, are positive spatial random stationary processes. The processes $D(x)$ and $k(x)$ are independent of each other (cross correlation equal to zero). The spatial variability of $k(x)$ implies the variability of the Langmuir maximum and will be referred to as Langmuir coefficient hereafter for simplicity. The typical forms of $f(u)$ are Langmuir isotherm: $u/(1+u)$; Freundlich isotherm: $u^p$, $0 < p < 1$; or convex isotherm: $u^p$, $p > 1$, see [6,11,12,15] for details. The spatial function $k(x)$ models the chemical (sorptive) heterogeneity of the soil columns due to the presence of macropores, aggregates, cracks, and rocks, etc. The spatial function $D(x)$ models the effects of advection and the heterogeneity in porous media. The self-adjoint form of the right hand side of (1.1) is also a useful way of writing the advection/diffusion operator $\Delta + w \cdot \nabla$, in several space dimensions, where $w$ is an incompressible mean zero stationary velocity field as often encountered in linear transport equations. Thus the form of the right hand side of (1.1) will help us gain insight for the future modeling of multidimensional problems.

Under constant input of $u$ at $x = -\infty$ into an initially solute-free column ($u = 0$), the dynamics of (1.1) are governed by moving random fronts, which are the main objects of our investigation here. The existence and asymptotic stability of traveling wave solutions to (1.1) are well-understood if $k(x)$ and $D(x)$ are equal to constants (homogeneous media), see [9,11,12]. More recently, the existence and asymptotic stability of traveling waves in periodic media (i.e., $k(x)$ and $D(x)$ are assumed to be positive periodic functions of $x$) have been studied in [15,16]. Solutions eventually approach spatially periodically varying traveling waves that move at constant averaged speed with initial data dependent phase shifts. What happens to the fronts in random media? Do they propagate? If so, what is the essential difference between fronts in periodic and random media?

It appears hard to approach the problem of large time front asymptotics in a mathematically rigorous way if $k(x)$ or $D(x)$ is a stationary random process. The major difficulty is that nonlinearity and randomness coexist in equation (1.1), and there seems to be no explicit formula for the solutions. However, we can indeed get some hints from recent rigorous results on random fronts of the solvable viscous Burgers equation. It is proved in [13] that when a viscous shock profile is initially perturbed by a Gaussian random field (in particular, white noise), then at large times, the solutions behave like fronts propagating with the unperturbed velocity in the sense of distribution. The front velocity is still given by the Rankine–Hugoniot relation since the governing equation remains a conservation law in the presence of randomness. However, the front location is random, and satisfies a central limit theorem with standard deviation of the order $O(\sqrt{t})$. That is to say, on the time scale $O(\sqrt{t})$ the front location minus its ensemble mean behaves like a Gaussian random variable. More precisely, let us denote by $u_s(x)$ the viscous shock profile of the Burgers equation

$$u_t + \left(\tfrac{1}{2}u^2\right)_x = \nu u_{xx}, \quad \nu > 0,$$

such that $u_s(-\infty) = 1$, $u_s(+\infty) = 0$. Let $V_x$ be a Gaussian process with enough

decay of correlations, and define front location as $z(t) = \min\{x\colon\ u(x,t) = \frac{1}{2}\}$. Then $z(t)$ is almost surely finite for large times, and there exists a constant $\sigma > 0$ such that

$$\frac{z(t) - t/2}{\sigma\sqrt{t}}$$

converges in distribution to the unit Gaussian random variable.

Recently, shock front speeds in an inviscid Burgers equation with random flux function of the form

$$u_t + \left(\tfrac{1}{2}a(x)u^2\right)_x = 0$$

were considered [14]. Here $a(x) > 0$ is a stationary process with fast decay of correlation, and finite ensemble mean of $1/a(x)$. The initial condition is the indicator function of the negative real axis. A similar central limit theorem is established for front location where $u$ drops from one to zero.

Is the story the same for fronts in random media governed by nonsolvable conservative PDEs? It is our goal to answer this question through accurate numerical simulation of the model equation (1.1). For convenience, we will concentrate on the Langmuir isotherm in this paper. The other forms of $f(u)$ can be studied in the same manner. The averaged front speed given by the Rankine–Hugoniot relation can be explicitly written down. The speed formula is known in the setting of periodic media [15], and we extrapolate it to random media. Suppose solution $u = u(x,t)$ approaches a constant state $u_\mathrm{l} > 0$ at $x = -\infty$ and another constant $u_\mathrm{r} \in [0, u_\mathrm{l})$ at $x = +\infty$. Such boundary data correspond to the situation of solute transport into less concentrated areas with water flow as studied in [2,10]. The wave speed denoted by $s$ is given by an averaged Rankine–Hugoniot relation:

$$s = \frac{v(u_\mathrm{l} - u_\mathrm{r})}{(u_\mathrm{l} + \langle k\rangle f(u_\mathrm{l})) - (u_\mathrm{r} + \langle k\rangle f(u_\mathrm{r}))} > 0, \tag{1.2}$$

which depends only on the expectation (or ensemble mean) of $k(x)$, denoted by $\langle k\rangle$.

Our main finding is that the *front location* $X(t)$ *defined as the leftmost point where* $u$ *is equal to* $(u_\mathrm{l} + u_\mathrm{r})/2$ is described by the following law:

$$\frac{(X(t) - st)}{\sqrt{t}} \sim \text{Gaussian}, \tag{1.3}$$

for large $t$, where the Gaussian random variable has zero mean and a standard deviation $\sigma > 0$. We found numerically an empirical formula for $\sigma$:

$$\sigma = \text{const}\,\sigma_k\sqrt{l_\mathrm{c}}, \tag{1.4}$$

where $\sigma_k$ is the standard deviation of the stationary process $k(x)$, and $l_\mathrm{c}$ the correlation length of the process $k(x)$. We then present a theory for the front fluctuation based on the rigorous results established for fronts in the solvable noisy Burgers equations [13,14]. The theory gives the formula

$$\sigma = f(u_\mathrm{l})\sigma_\mathrm{a}\sqrt{2s}, \tag{1.5}$$

where $\sigma_{\mathrm{a}}$ is the velocity autocorrelation (see 4.3) of the process $k(x)$, and $s$ is the mean front speed given by (1.2). Using the specific statistics of $k(x)$ used in the simulations, we derive formula (1.4) from formula (1.5), achieving spectacular agreement between theory and numerics.

The significant difference between deterministic fronts in periodic media and random fronts is that random fronts can not stabilize towards a constant speed motion. Instead, fronts move at a constant speed in the background of noise with a standard deviation of order $\mathrm{O}(\sqrt{t})$. The random noise persists in time. Our numerical computation suggests that it satisfies a central limit theorem in the large time limit.

In [2] the authors numerically studied the traveling fronts of (1.1) in the case of Freundlich nonlinearity $f(u) = u^p$, $p \in (0, 1)$. They used the so called moment methods to calculate the mean front location and the width of fronts. The moment method regards $-u_x$ as a probability density function (strictly speaking $u_x$ does not have a distinguished sign in the inhomogeneous media and hence may not be defined as a density), and uses the space integral of powers of $x$ times $-u_x \,\mathrm{d}x$ to calculate front location and front widths, etc. The advantage of this method is that one does not have to capture the front location. The drawback, however, is that spatial integration corresponds to some kind of averaging (same as the ensemble average when ergodicity holds), and therefore is not desirable for studying front fluctuations. Indeed, the authors of [2] were most concerned with average speed and averaged front shape (over 600 samples). Due to the inherent averaging effects of the method, and the additional average over samples, the front widths turn out much larger than those of individual realizations. In some parameter regimes, the front widths grow with time like $\mathrm{O}(t^2)$ (see [2, (37b), p. 128]).

Our simulation is based on capturing the front location $X(t)$ for each realization and studying its statistics over larger numbers of samples. We calculate the (leftmost) point of the level set $u = (u_{\mathrm{l}} + u_{\mathrm{r}})/2$ individually, then average over 1000 samples to get the mean front position. Next, we subtract off the mean from each sample, and compute the standard deviation. Finally, we carry out chi-square tests on the Gaussian noise. Our approach is better for checking the validity of the ansatz (1.3). We also perform sample average over front profiles; however, we have not observed front spreading as much as $\mathrm{O}(t^2)$. We found the interesting phenomenon that the numerically computed standard deviation of random fronts is much less sensitive to the grid refinement than the front mean position is.

The rest of the paper is organized as follows. In section 2, we describe our numerical scheme and numerical construction of random processes $k(x)$ and $D(x)$. In section 3, we present our numerical results on random fronts and the statistical tests performed to verify the Gaussian hypothesis. In section 4, we present the theory of front fluctuation based on the mass conservation principle which is behind the results in [13,14]. We derive the front standard deviation formulas (1.5) and (1.4). The concluding remarks are in section 5.

## 2. Numerical scheme and random process

### 2.1. Discretization of the transport equation

Because we want to study the long term behavior of the concentration we choose to solve equation (1.1) in the moving frame coordinates with the speed $s$ given by (1.2). We will therefore compute $\omega(y,t) = u(x,t)$ with $y = x - st$. Equation (1.1) becomes

$$\begin{aligned}&\partial_t\big(\omega(y,t) + k(y+st)f\big(\omega(y,t)\big)\big)\\&\quad = \partial_y\big(D(y+st)\partial_y\omega(y,t)\big) - (v-s)\partial_y\omega(y,t) + s\partial_y\big(k(y+st)f\big(\omega(y,t)\big)\big),\\&\omega(-\infty,t) = u_{\mathrm{l}}, \quad \omega(+\infty,t) = u_{\mathrm{r}}.\end{aligned} \tag{2.1}$$

In moving frame coordinates we reduce the space domain to a slab of length $L$ centered around the initial position of the shock and use the Neumann boundary condition at each end of this slab. We discretize the slab in $N+1$ intervals of length $\delta_y = L/(N+1)$ and denote by $\delta_t$ the time sample. We can now write the discretized scheme for the full equation (2.1) using standard notations $\omega_i^n = \omega(i\delta_y, n\delta_t)$, $k_i^n = k(i\delta_y + sn\delta_t)$ and $D_i^n = D(i\delta_y + sn\delta_t)$, $1 \leqslant i \leqslant N$. The time derivative is discretized by a forward finite difference of order one, and the discretization of the diffusion and convection terms is fully implicit. The convection term is discretized using a backward (upwind) finite difference in space:

$$\begin{aligned}&\omega_i^{n+1} + k_i^{n+1}f\big(\omega_i^{n+1}\big) - \omega_i^n - k_i^n f(\omega_i^n)\\&\quad = \delta_t\Bigg\{\frac{D_{i+1}^{n+1}\omega_{i+1}^{n+1} - (D_{i+1}^{n+1} + D_i^{n+1})\omega_i^{n+1} + D_i^{n+1}\omega_{i-1}^{n+1}}{\delta_y^2} - (v-s)\frac{\omega_i^{n+1} - \omega_{i-1}^{n+1}}{\delta_y}\\&\qquad + s\,\frac{k_i^{n+1}f(\omega_i^{n+1}) - k_{i-1}^{n+1}f(\omega_{i-1}^{n+1})}{\delta_y}\Bigg\}\end{aligned}$$

for $1 < i < N$. Discretization of order $\mathrm{O}(\delta_y)$ of the Neumann boundary condition provides $\omega_0^n = \omega_1^n$ and $\omega_{N+1}^n = \omega_N^n$ for all times $n$. We can rewrite the scheme in a compacter fashion

$$\boldsymbol{T}^{n+1}\boldsymbol{\omega}^{n+1} + \big(\boldsymbol{K}^{n+1} - \boldsymbol{B}^{n+1}\big)\boldsymbol{f}^{n+1} = \boldsymbol{\omega}^n + \boldsymbol{K}^n\boldsymbol{f}^n$$

with $\boldsymbol{T}^n$ the tridiagonal matrix such that

$$\boldsymbol{T}^n = \begin{bmatrix} 1 + \frac{\delta_t D_2^n}{\delta_y^2} & -\frac{\delta_t D_2^n}{\delta_y^2} & \\ -\frac{\delta_t}{\delta_y}\Big(\frac{D_1^n}{\delta_y} + v - s\Big) & 1 + \frac{\delta_t}{\delta_y}\Big(\frac{D_{i+1}^n + D_i^n}{\delta_y} + v - s\Big) & -\frac{\delta_t D_{i+1}^n}{\delta_y^2} \\ & -\frac{\delta_t}{\delta_y}\Big(\frac{D_N^n}{\delta_y} + v - s\Big) & 1 + \frac{\delta_t}{\delta_y}\Big(\frac{D_N^n}{\delta_y} + v - s\Big) \end{bmatrix}. \tag{2.2}$$

$\boldsymbol{K}^n$ is the diagonal matrix of components $\boldsymbol{K}^n_{ii} = k^n_i$, $\boldsymbol{B}^n$ is a bidiagonal inferior matrix

$$\boldsymbol{B}^n = \begin{bmatrix} \frac{\delta_t}{\delta_y}\big(k^n_1 - k^n_0\big)s & & \\ -\frac{\delta_t}{\delta_y}k^n_{i-1}s & \frac{\delta_t}{\delta_y}k^n_i s & \\ & -\frac{\delta_t}{\delta_y}k^n_{N-1}s & \frac{\delta_t}{\delta_y}k^n_N s \end{bmatrix} \tag{2.3}$$

and $\boldsymbol{\omega}^n$ (resp. $\boldsymbol{f}^n$) is the vector of components $\omega^n_i$ (resp. $f(\omega^n_i)$). To treat the nonlinear term $\boldsymbol{f}^n$ we use a generalized Newton method. Denoting by $\widetilde{\boldsymbol{\omega}}^n$ an approximation of $\boldsymbol{\omega}^n$ we have that

$$\boldsymbol{f}^n_i = f\big(\widetilde{\omega}^n_i\big) + \big(\omega^n_i - \widetilde{\omega}^n_i\big) f'\big(\widetilde{\omega}^n_i\big).$$

We denote by $\boldsymbol{\omega}^n_m$ the successive approximations of $\boldsymbol{\omega}^n$ starting with $\boldsymbol{\omega}^n_0 = \boldsymbol{\omega}^{n-1}$ and we know that $\boldsymbol{\omega}^n_m \to \boldsymbol{\omega}^n$ as $m \to \infty$ if $\boldsymbol{\omega}^{n-1}$ is close enough to $\boldsymbol{\omega}^n$, that is, if $\delta_t$ is sufficiently small.

We are left with the iterative scheme

$$\begin{aligned} &\big(\boldsymbol{T}^{n+1} + \big(\boldsymbol{K}^{n+1} - \boldsymbol{B}^{n+1}\big)\boldsymbol{f'}^{\,n+1}_m\big)\boldsymbol{\omega}^{n+1}_{m+1} \\ &\quad = \boldsymbol{\omega}^n + \boldsymbol{K}^n\boldsymbol{f}^n + \big(\boldsymbol{K}^{n+1} - \boldsymbol{B}^{n+1}\big)\big(\boldsymbol{f'}^{\,n+1}_m\boldsymbol{\omega}^{n+1}_m - \boldsymbol{f}^{n+1}_m\big), \end{aligned}$$

where $\boldsymbol{f'}^{\,n}_m$ is the diagonal matrix of diagonal component $f'(\omega^n_{i\,m})$.

Numerical accuracy is very important in our experiments because we want to study the long term behavior of the shock. In the moving frame, we expect the position of the shock to vary very little, or at least to vary around a mean position constant with time which should be the initial position. There are several ways of verifying this. Since we use a conservative scheme, the total mass in the moving frame coordinates should remain constant. It is a necessary condition but does not give much information about the shape of the moving front. We choose to measure the position of the shock by the position of its midpoint, i.e., the abscissa at which the value of the function equals $0.5(u_\mathrm{l} + u_\mathrm{r})$. This is a little arbitrary in the sense that even for homogeneous coefficients this abscissa varies a little with time. The diffusion term modifies the shape of the initial front, and the discretization of space derivatives cannot ensure that this modification is symmetrical about the initial shape. We will illustrate the influence of the discretization on the front position in the next section.

### *2.2. Simulation of the random coefficients*

In equation (2.1) the coefficients $k(y)$ and $D(y)$ are random processes of the variable $y$. As has been explained in sections 1 and 2, the shock is expected to propagate with a mean speed $s$,

$$s = \frac{v(u_\mathrm{l} - u_\mathrm{r})}{u_\mathrm{l} - u_\mathrm{r} + \langle k\rangle(f(u_\mathrm{l}) - f(u_\mathrm{r}))}, \tag{2.4}$$

where $\langle k\rangle$ is the statistical mean of the random Langmuir coefficient. We also expect the shock to behave asymptotically as a Gaussian variable, and its variance should therefore increase linearly with $\sqrt{t}$. The dependence of the variance with respect to other factors, such as the variance and the correlation length of the coefficients $k$ and $D$, is not known theoretically, and can only be illustrated with numerical simulations. In the following, $\langle\cdot\rangle$ refers to the statistical mean of a random variable and is estimated and represented in the various figures with the following conventions:

$$\text{mean } \langle X\rangle \approx \frac{1}{N}\sum_{i=1}^{N} X^i,$$

where $X^i$ is the $i$th realization out of $N$ of the random variable $X$. The variance and covariance are defined as

$$\text{variance } \big\langle \big(X-\langle X\rangle\big)^2\big\rangle \approx \frac{1}{N-1}\sum_{i=1}^{N}\big(X^i-\big\langle X^i\big\rangle\big)^2,$$

$$\begin{aligned}\text{covariance } C_n &= \big\langle \big(X_j-\langle X\rangle\big)\big(X_{j+n}-\langle X\rangle\big)\big\rangle \\ &\approx \frac{1}{(N-1)(L-n)}\sum_{i=1}^{N}\sum_{k=0}^{L-n}\big(X_k^i-\langle X\rangle\big)\big(X_{k+n}^i-\langle X\rangle\big),\end{aligned}$$

where $X_k^i$ is the $k$th sample of the $i$th realization of a random process $X_k$. The latter formula is used for stationary $X_k$ where $C_n$ does not depend on $j$. For estimation, the mean defined above is used in lieu of $\langle X\rangle$.

We build correlated random processes using independent identically uniformly distributed random variables $\eta_i$ and $\gamma_i$. At a given index $i$, the random variable $\eta_i$ has mean $\langle\eta\rangle$ and standard deviation $\sigma_\eta$ and is uniformly distributed in the interval $[\langle\eta\rangle-\sqrt{3}\sigma_\eta, \langle\eta\rangle+\sqrt{3}\sigma_\eta]$. The coefficients $k_i$ and $D_i$ are constructed in the following way:

$$\begin{aligned}k_i &= \beta k_{i-1}+\eta_i,\\ D_i &= \beta D_{i-1}+\gamma_i,\end{aligned} \tag{2.5}$$

where $\beta\in(0,1)$. It is easy to verify that

$$\begin{aligned}\sigma_\eta^2 &= \sigma_k^2\big(1-\beta^2\big) \quad\text{and}\quad \sigma_\gamma^2 = \sigma_D^2\big(1-\beta^2\big),\\ \langle\eta\rangle &= \langle k\rangle(1-\beta) \quad\text{and}\quad \langle\gamma\rangle = \langle D\rangle(1-\beta).\end{aligned}$$

The correlation function of $k_i$ is $\langle(k_i-\langle k\rangle)(k_{i+n}-\langle k\rangle)\rangle\sigma_k^{-2}=\beta^n$. The standard definition of the correlation length $l_c$ of a stationary random sequence $\mu_i$ is the non-dimensional number appearing in the correlation:

$$\big\langle\big(\mu_i-\langle\mu\rangle\big)\big(\mu_{i+n}-\langle\mu\rangle\big)\big\rangle\sigma_\mu^{-2}=\exp\{-n/l_c\}.$$

Here, we take into account the dimension of the problem in the sense that $k_i = k(i\delta_{\mathrm{r}})$, hence the correlation length

$$l_{\mathrm{c}} = \frac{-\delta_{\mathrm{r}}}{\log \beta},$$

where $\delta_{\mathrm{r}}$ is the space step between two consecutive random samples.

Such correlated samples are constructed for instance in [2]. To improve its statistics, a base correlated sample is generated with a certain sampling rate $Dz^*$, which is then used only once every $X$ points (with $X$ natural integer). This amounts to a discretization step $Dz = XDz^*$. At each discretization point the random value from the initial sample is used – simply dropping the intermediate points.

We do not use exactly this model, because the finite difference scheme requires the coefficients to be smooth. For simplicity, this requirement is reduced in practice to the continuity achieved by linear interpolation at the intermediate computation points. If there are $M$ discretization points spaced by $\delta_y$ between two consecutive random values spaced by $\delta_{\mathrm{r}} = M\delta_y$, the coefficient $k$ is given at the discretization point $i\delta_y$ by

$$k(i\delta_y) = \frac{([i/M]+1)\delta_r - i\delta_y}{\delta_r} k_{[i/M]} + \frac{i\delta_y - [i/M]\delta_r}{\delta_r} k_{[i/M]+1}$$
$$\text{for } [i/M]\delta_r \leqslant i\delta_y < \big([i/M]+1\big)\delta_r, \tag{2.6}$$

and the diffusion is obtained similarly. One sees the effect of this linear interpolation on the covariance function in figure 1. It modifies the shape of the covariance function for small lag (left-hand side graph), but does not modify the exponential asymptotic decay (right-hand side graph). The curve labelled $0.003\exp(-x)$ shows the theoretical covariance function for a unit correlation length. The simulations are done using a sample $\delta_y = 0.012$ and three different spacings between two correlated random samples $\delta_{\mathrm{r}} = 20\delta_y$, $10\delta_y$ and $\delta_y$, corresponding to the three graphs labelled “20 pts”, “10 pts”

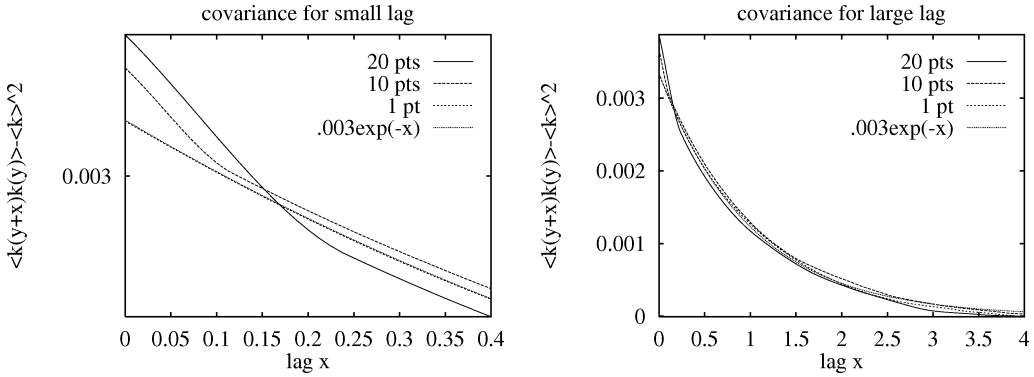


Figure 1. Covariance function for the random coefficients.

and "1 pt". The covariance estimates are obtained by averaging over five hundred independent realizations of the processes given by (2.5).

Note that this definition of the correlation length is not to be mistaken for the correlation length of locally correlated random processes. There are many ways to construct such processes. Piecewise constant processes whose consecutive values are independent random variables are locally correlated with a correlation length equal to the average length where the function is constant. For piecewise linear processes whose consecutive local extrema are independent random variables, the correlation length is twice the average distance between two local extrema. In both cases, the correlation between two samples drops to zero as soon as they are further apart than one correlation length. With the random processes we use here, this is not the case. The correlation length quantifies the exponential decay of the correlation. As one can see on the right-hand side of figure 1 the correlation is still one third of its maximum for samples that are one correlation length apart.

## 3. Numerical results on random fronts

With correlated random coefficients $k$ and $D$ constructed according to (2.5) and (2.6), we simulate the propagation of the shock for different values of the correlation length and variance. We use the moving frame scheme described in the previous section and place the shock initially at position $x_{\text{shock}}(t = 0) = 8$. The space range goes from $y = 0$ to $y = 17.5$ discretized with 700 space grids with $\delta_y = 0.025$. The random coefficients have mean $k_{\text{m}} = 1$, $D_{\text{m}} = 0.02$ and standard deviation $k_{\text{dev}} = 0.29$, $D_{\text{dev}} = 0.0057$. There are five space grids between two consecutive random coefficients. The shock is propagated from time 0 until time $t = 200$, over 2000 time steps of length $\delta_t = 0.1$ with a constant water velocity $v = 1$. At each time step, the new position of the shock $x_{\text{shock}}(t)$ is defined as the abscissa at which the solution equals $0.5(u_{\text{l}} + u_{\text{r}})$ and is computed by linear interpolation between the two nearest samples.

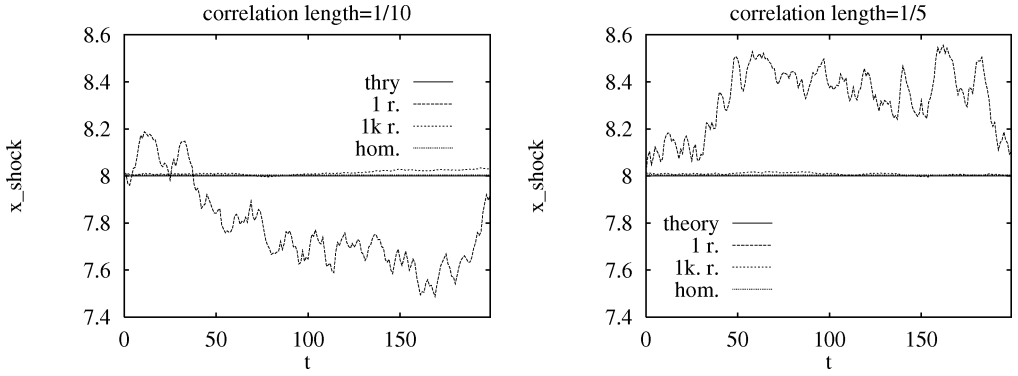


Figure 2. Position of the shock for correlation lengths $1/5$ and $1/10$.

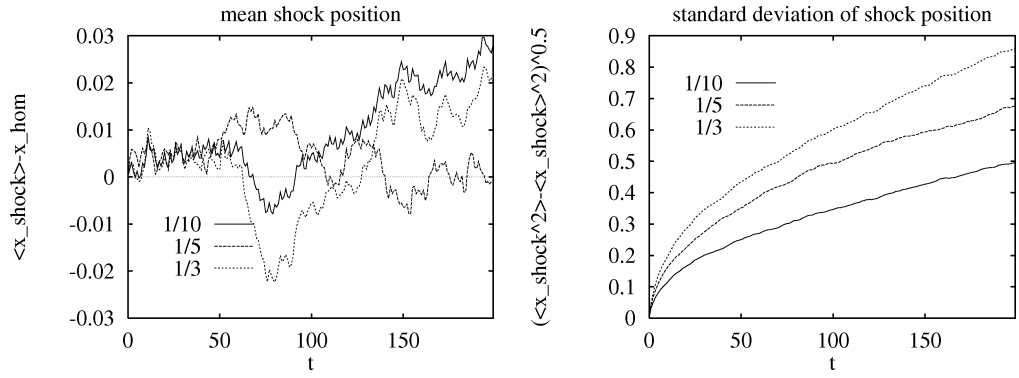


Figure 3. Mean and variance of the shock position for correlation lengths $1/5$ and $1/10$.

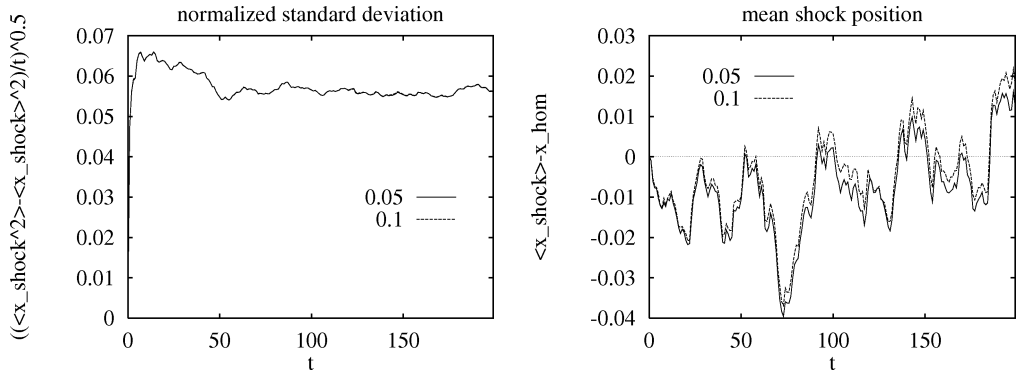


Figure 4. Influence of discretization on the mean and standard deviation of the shock position. Averages over 200 realizations.

In figure 2, the position of the shock is represented as a function of time, for two correlation lengths, $1/10$ on the left-hand side and $1/5$ on the right-hand side. In each figure the shock position for a single realization (label "1 r.") is plotted along with the mean, – averaged over 1000 realizations (label "1k r."), the theoretical value ($x_{\text{shock}} = 8$, label "thry") and the value computed with homogeneous coefficients (label "hom"). The shock position in the case of homogeneous coefficients remains stable after a short initial phase, and is very close to the theoretical one. This is normal since we use the shock at time $t = 0$ as initial data for the equation in the moving average equation, which is valid only after the propagation has reached its stationary regime.

On the left- (resp. right-) hand side of figure 3 the mean $\langle x_{\text{shock}} \rangle$ (resp. standard deviation $(\langle x_{\text{shock}}^2 \rangle - \langle x_{\text{shock}} \rangle^2)^{0.5}$) of the shock position $x_{\text{shock}}(t)$ computed over 1000 independent realizations is represented as a function of time, for correlation lengths $1/10$, $1/5$ and $1/3$. The left-hand side curves exhibit a small drift in the mean position – which should be constant since we work in the moving average frame. It seems to be mostly due to the discretization. In figure 4, we compare the results obtained with ($\delta_t = 0.1$, $\delta_y = 0.025$) (which is the discretization used in all the other figures),

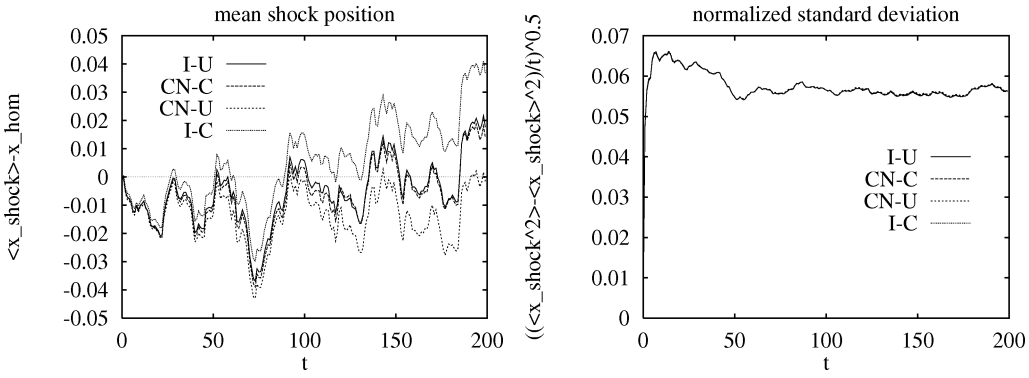


Figure 5. Comparison of different numerical schemes on the mean and normalized standard deviation of the shock position. Averages over 200 realizations. Coarse discretization.

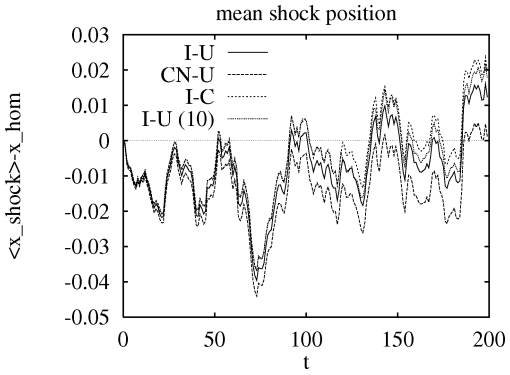


Figure 6. Comparison of different numerical schemes on the mean of the shock position. Averages over 200 realizations. Fine discretization.

and ($\delta_t = 0.05$, $\delta_y = 0.0125$) for the one third correlation length. The statistics are estimated using 200 realizations. Both the standard deviation and the mean seem to be accurately computed with our discretization. There are small discrepancies in the mean position of the order of $\delta_y/10$ after 2000 time steps. In figure 5, we compare the results obtained with different numerical schemes for the same correlation length. The reference scheme (I-U) is the one used in all others computations: fully implicit, with an upwind discretization of the residual convection term and a Neumann boundary condition on the right-hand side. Were the coefficients smooth, improvements could be theoretically expected by using a Crank–Nicholson scheme instead of the fully implicit, a centered finite difference instead of the upwind scheme, or a homogeneous Dirichlet boundary condition instead of the Neumann one. We combine the different possibilities to try three other schemes: (CN-U) Crank–Nicholson and upwind convection term, (CN-C) Crank–Nicholson but with a centered discretization of the convection term, and eventually (I-C), fully implicit but a centered convection discretization. Here, the performances of the different schemes are identical as far as the variance is concerned,

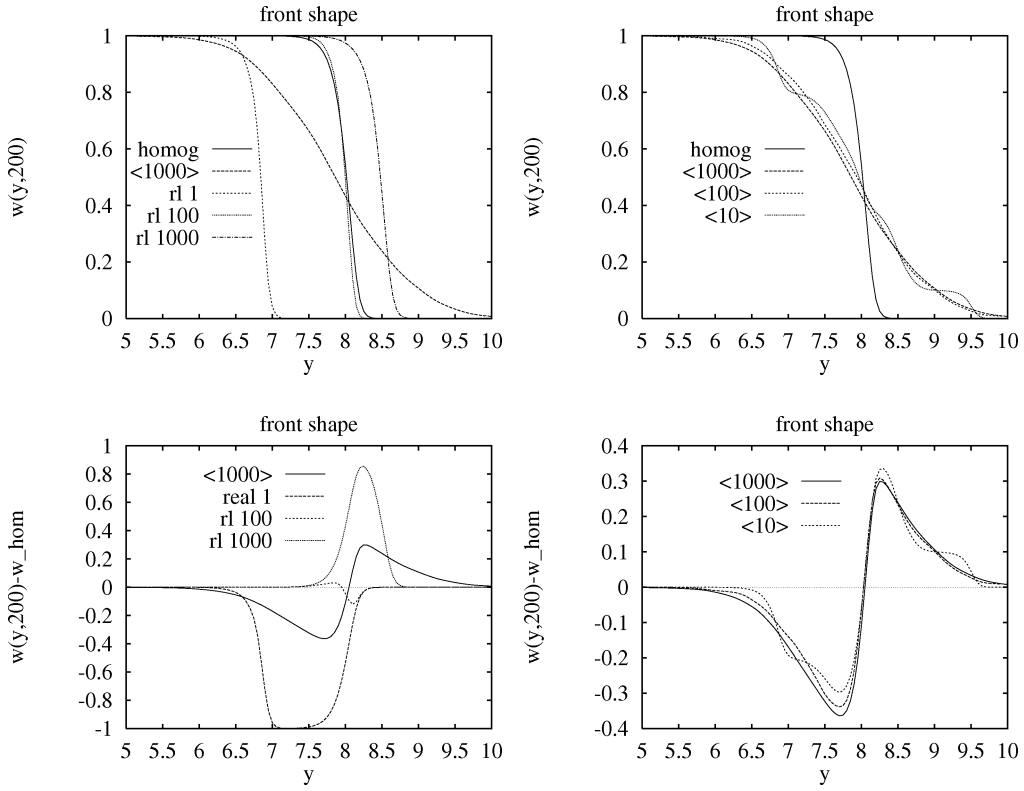


Figure 7. Influence of randomness on front shape.

and comparable up to the order of the space discretization in the case of the shock position itself. Figure 6 shows the same comparison but with the finer discretization ($\delta_t = 0.05$, $\delta_y = 0.0125$). The discrepancies between the different schemes are smaller than in figure 5 corresponding to the ($\delta_t = 0.1$, $\delta_y = 0.025$) discretization.

In the different simulations, the variance of the shock position seems to stabilize very quickly with respect to the discretization parameters. On the other hand, the influence of the correlation length and the discretization on the mean shock position appear to be quantitatively comparable. In fact the mean shock position is theoretically constant and does not depend on the correlation length. The variation exhibited by the numerical simulations can be explained by the fact that changing the correlation changes the variation rate of the Langmuir and diffusion coefficient, i.e., the larger the correlation rate the smoother the coefficient. The smoothness of the coefficients is of course directly linked to the level of numerical accuracy.

One should not expect to recognize the presence of randomness by looking at a single realization of the front. The speed of the front varies in time around the mean speed but at a given time, the shape of the shock is very much the same as if it had propagated in a homogeneous medium. On the other hand, because each realization moves with a different speed, the effect of randomness on the average front shape

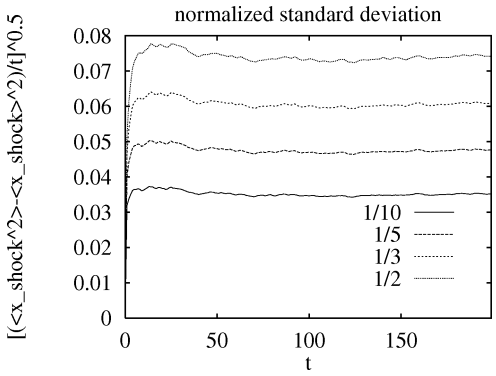


Figure 8. Influence of the correlation length of the Langmuir coefficient on the standard deviation of the shock position.

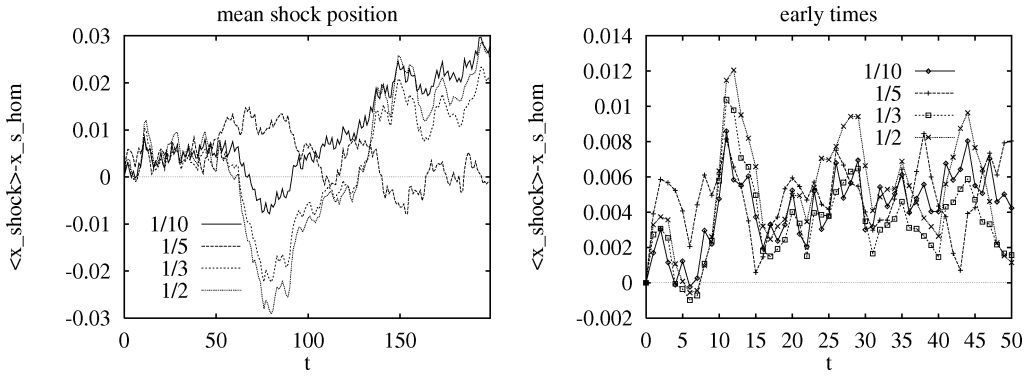


Figure 9. Influence of the correlation length on the mean shock position.

– averaged over many realizations – is to widen the front. Averaging on a small number of realizations – 10 for instance – will give a widened front with ripples. To illustrate this, figure 7 shows on the left-hand side three different single realizations of the shock at time $t = 200$, along with the homogeneous shock, and the average over 1000 realizations. On the right-hand the shock is averaged over 10, 100 and 1000 realizations. The upper figures show the shocks, the lower ones show the shocks minus the homogeneous one. For these figures, the correlation length is $1/3$.

We turn next to the verification of our main hypothesis, which is that the shock position behaves like a Gaussian variable at large times. First of all we check that the standard deviation exhibits the correct behavior in time. In figure 8 the standard deviation of the shock position normalized by $\sqrt{t}$ is represented as a function of time for Langmuir coefficients with four different correlation lengths. In figure 9, the corresponding mean shock positions (relative to the homogeneous value) are shown for the four correlation lengths. The variance is estimated using 1000 realizations for the four curves that stabilize quickly – after a few correlation lengths. The standard deviation of the position of the shock depends on time, with the expected growth rate

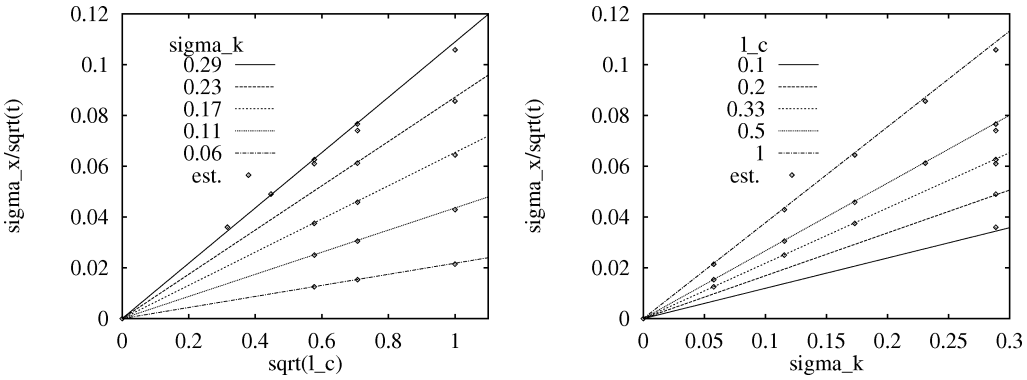


Figure 10. Influence of the standard deviation and correlation length of the Langmuir coefficient on the standard deviation of the shock position.

in $\sqrt{t}$. It seems also to depend on the standard deviation and the correlation length of the Langmuir coefficient as

$$\sigma_x = c\sigma_k\sqrt{l_c t}, \tag{3.1}$$

where $c$ is an absolute constant. We verify this formula numerically. The constant $c$ in the formula is estimated by averaging over all the simulations performed for five different values of $l_c$ from 1 to 0.1 and five different values of $\sigma_k$. The results are summarized in figure 10 for a value of the constant found approximately equal to $c = 2.65$. On the left-hand side the variations of the standard deviation normalized by $\sqrt{t}$ are shown as a function of the square root of the correlation length of $k$ for different values of the standard deviation of $k$. The right-hand side shows the dependence with respect to the standard deviation. The lines are according to the above formula, and the symbols are estimates from the data.

Finally, we perform the well known $\chi^2$-test to corroborate the Gaussianity of the position of the shock. The shock position at a given time is first centered and normalized by its standard deviation. Since the numerical experiments exhibit a slight deviation of the computed mean with respect to its theoretical value, we do not assume stationarity but estimate the mean at each time and use this estimate to center the data. On the other hand, the standard deviation seems to obey the expected behavior quite well asymptotically. We therefore compute – using all the times after the transition phase – an estimate of the coefficient $c$ such that the standard deviation $\sigma_x = c\sqrt{t}$ and use it to normalize the data by $\sigma_x$.

The range of the normalized and centered shock position at a given time is divided into $k$ mutually exclusive sets

$$A_1 = (-\infty, a_1], \quad A_2 = (a_1, a_2], \quad \ldots, \quad A_k = (a_{k-1}, \infty).$$

Let

$$p_j = P(A_j) = \frac{1}{\sqrt{2\pi}} \int_{a_{j-1}}^{a_j} \exp\{-0.5x^2\}\,\mathrm{d}x \tag{3.2}$$

denote the probability that the computed shock position will fall in the $j$th interval after centering and normalization. For a sample of size $N_{\text{real}}$ obtained by computing $N_{\text{real}}$ independent realizations of the shock propagation, the expected number of observations to occur in $A_j$ is $e_j = N_{\text{real}}\, p_j$. Following [4], we choose a priori the number of intervals $A_j$ and eventually combine those with too small $e_j$ values so that all $e_j$ are greater than 5. In the test presented here, we start with 20 intervals of equal width $l$ such that $L = 20l = 6$. We perform the test with $N_{\text{real}} = 1000$ and the lower limit of 5 for $e_j$ reduces the number of intervals to $k = 18$.

To measure the agreement between the expected values and the sample measurements we compute the statistic

$$u = \sum_{j=1}^{k} \frac{(O_j - e_j)^2}{e_j},$$

where $O_j$ denotes the number of shock position in cell $A_j$. The probability $p$ that the hypothesis is verified is computed using the incomplete $\Gamma$ function

$$p = P\big[\chi^2 > u \mid k - 1 - n_{\text{c}}\big] = \frac{1}{\Gamma(k-1-n_{\text{c}})} \int_u^{\infty} \mathrm{e}^{-t} t^{k-2-n_{\text{c}}}\,\mathrm{d}t, \tag{3.3}$$

where $n_{\text{c}}$ is the "number of constraints". One constraint comes from estimating the mean from the data itself instead of using the theoretical value. On the other hand, we use all times to compute the standard deviation, based on the numerically verified relation $\sigma_x = c\sqrt{t}$. Therefore the value of $\sigma_x$ that we use at a single time to normalize the data and perform the $\chi^2$-test depends only fractionally on the tested data and we let $n_{\text{c}} = 1$.

Note that a good agreement – i.e., a high probability $p$ – does not ensure that the hypothesis is true. On the other hand, if they do not agree the Gaussian hypothesis should be rejected.

Figure 11 shows histograms at two different times where the data met the 10% and 90% levels of the $\chi^2$-test. The curves on the left-hand side (respectively right-hand side) correspond to $O_i$ and $e_j$ leading to $p = 0.1$ (resp. $p = 0.9$) in (3.3). The symbols on the curves indicate the locations of the 18 binning intervals.

Figure 12 corresponds to the shock position in a random medium with a correlation length $l_{\text{c}} = 0.5$ and a standard deviation $\sigma = 0.29$. It shows the corresponding probabilities as a function of time – that is, the level at which the Gaussian hypothesis should be rejected. The horizontal line at $p = 0.1$ indicates the 10% test level. The Gaussian hypothesis should be rejected at the 10% level for all times where $p$ is below this line. In other words, if the samples are uncorrelated in time and normally distributed, one can expect 10% of them to fall below this line. The curves on the

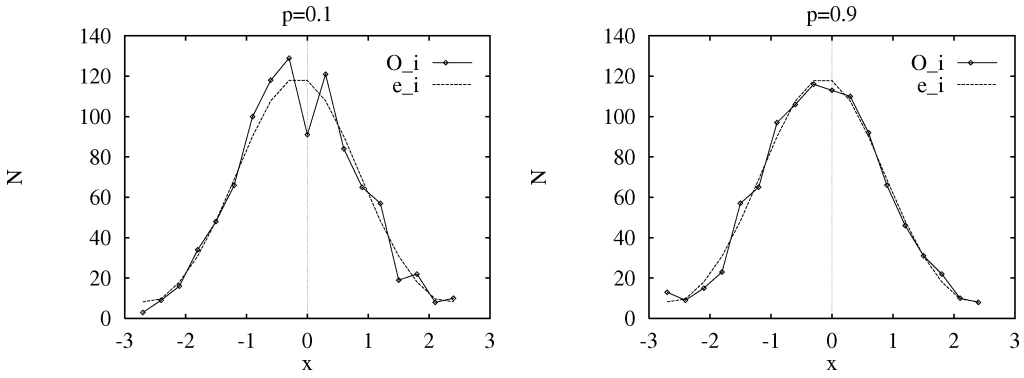


Figure 11. Histograms of the $\chi^2$-test at the 10% and 90% levels.

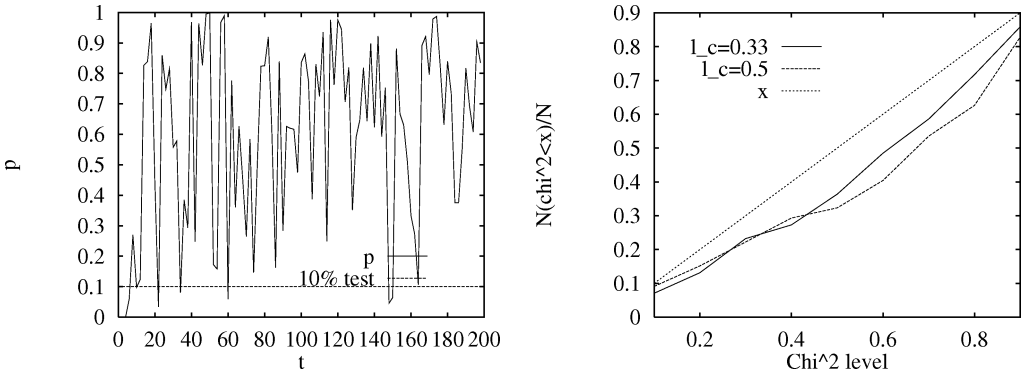


Figure 12. $\chi^2$-test for the shock position over 1000 realizations and 18 binning intervals.

right-hand side of figure 12 show the percentage of times at which the data fails a given level of the $\chi^2$-test. Were the data uncorrelated in time and ideally Gaussian, the curve should lie on the diagonal $p = x$. In all our simulations, the curves lie below the diagonal, as shown in the figure for two correlation lengths, 0.33 and 0.5. Since our data is obviously correlated in time, the only conclusion which can be drawn from these curves is that the Gaussian hypothesis cannot be rejected – as it should be if the curves were above the diagonal.

Finally, we also observe within the parameter range of our simulation that reducing the randomness ($D_{\text{dev}}$) in $D(x)$ all the way to constant $D$ causes no appreciable change to the above results on the statistical front asymptotics. The randomness in $k(x)$ is dominant. This is illustrated in figure 13, where the influence of the diffusion randomness on the mean shock position is seen by comparing two sets of simulations done with different randomness levels of the Langmuir coefficient and averaged over 10 independent realizations. The left-hand side curves are obtained with $k_{\text{dev}} = 0.29$. One curve corresponds to a constant diffusion (label "D=0.1"), the other one (labelled "Ddev=0.03") to a random diffusion of mean 0.1 and standard deviation $D_{\text{dev}} = 0.03$.

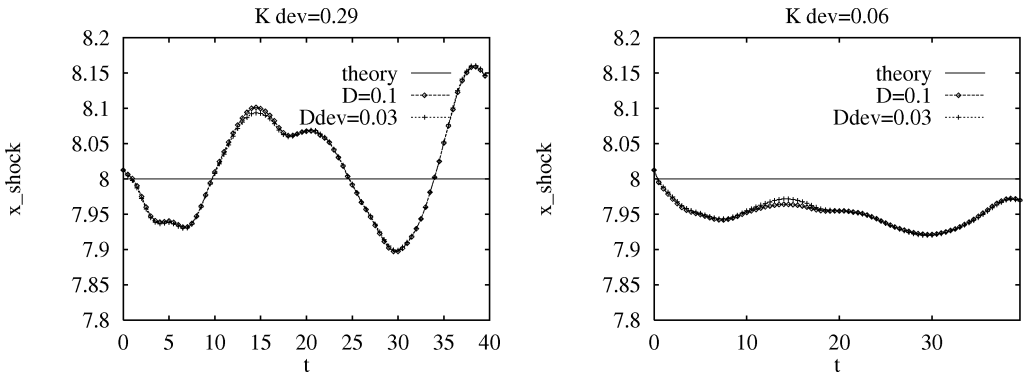


Figure 13. Influence of diffusion randomness on the mean of shock position.

In the right hand frame, the standard deviation of the Langmuir coefficient is smaller, $k_{\text{dev}} = 0.06$. The diffusion randomness seems to have only minor influence upon the results at an intermediate time interval. Otherwise, the curves look the same.

## 4. A theory of front fluctuation

In this section, we will derive the front standard deviation formula (3.1) discovered numerically in the last section.

To fix ideas, let us recall the result of [13] on the Burgers equation ($u_t+(u^2/2)_x = \nu u_{xx}$) with initial data being traveling front (connecting one at the left real line to zero at the right) plus white noise initial perturbation denoted by $V_x$. The intuition behind the rigorous result in [13] is that the front deviation from the mean location is approximately equal to the integral of white noise over the time interval $[-t/2, t/2]$, which gives $\sqrt{t}$ times unit Gaussian in law. This is an extension of the classical deterministic result [7] that the large time front phase shift is equal to the total mass of the initial (integrable) perturbation, as a direct consequence of the fact that *the integral of $u$ (mass) is a conserved quantity. The $\frac{1}{2}$ here is the mean front velocity of the unperturbed Burgers front.*

Back to equation (1.1), where *the $\int_{\mathbb{R}^1} u + k(x)f(u)$ is a conserved quantity*. Assume that $u_{\text{r}} = 0$. The mass density behind the front is $u_{\text{l}} + k(x)f(u_{\text{l}})$, which can be written as

$$u_{\text{l}} + \langle k\rangle f(u_{\text{l}}) + \big(k(x) - \langle k\rangle\big) f(u_{\text{l}}),$$

mean plus fluctuation. Let $s$ be the mean front velocity. By analogy with the Burgers equation, the front deviation is approximately equal to

$$\int_{-st}^{st} \big(k(x) - \langle k\rangle\big) f(u_{\text{l}})\,\mathrm{d}x. \tag{4.1}$$

For a stationary process with enough decay of correlations, the invariance principle holds (see [1]) and gives

$$\frac{\int_{-st}^{st}(k(x)-\langle k\rangle)\,\mathrm{d}x}{\sigma_{\mathrm{a}}\sqrt{2st}} \to W_1, \tag{4.2}$$

in law as $t \to +\infty$, where $W_1$ is the unit Gaussian, and $\sigma_{\mathrm{a}}$ is the velocity autocorrelation defined as

$$\sigma_{\mathrm{a}}^2 = \int_{-\infty}^{\infty} E\big[\big(k(0)-\langle k\rangle\big)\big(k(x)-\langle k\rangle\big)\big]\,\mathrm{d}x. \tag{4.3}$$

We have the formula

$$\sigma_x = f(u_{\mathrm{l}})\sigma_{\mathrm{a}}\sqrt{2st},$$

for large times. Or the root $t$ normalized front standard deviation $\sigma$:

$$\sigma = \lim_{t\to\infty}\frac{\sigma_x}{\sqrt{t}} = f(u_{\mathrm{l}})\sigma_{\mathrm{a}}\sqrt{2s}, \tag{4.4}$$

which is (1.5) in the introduction.

Now recall that the covariance function of (the discrete) $k$ is $\langle(k_0-\langle k\rangle)(k_n-\langle k\rangle)\rangle = \sigma_k^2\beta^n$, $n \geqslant 0$. Summing over $n$ gives

$$\sigma_{\mathrm{a}}^2 = \frac{\sigma_k^2}{(1-\beta)},$$

which is approximately equal to

$$-\frac{\sigma_k^2}{\log\beta},$$

for $\beta$ near 1 (as figure 1 suggests). Using the correlation length $l_{\mathrm{c}}$ of $k$, we can write the above as

$$\sigma_{\mathrm{a}}^2 = \frac{\sigma_k^2 l_{\mathrm{c}}}{\delta_{\mathrm{r}}},$$

where $\delta_{\mathrm{r}}$ is the spacing between two random samples, taken as $5\delta_y = 0.06$ in the simulation. We finally conclude that

$$\sigma_x = f(u_{\mathrm{l}})\sqrt{2s\delta_{\mathrm{r}}^{-1}}\sigma_k\sqrt{l_{\mathrm{c}}t} = \text{const}\ \sigma_k\sqrt{l_{\mathrm{c}}t}, \tag{4.5}$$

where the constant prefactor is $0.5\sqrt{2s(0.06)^{-1}}$ ($u_{\mathrm{l}} = 1$, $f(u_{\mathrm{l}}) = 0.5$). In the simulation, $\langle k\rangle = 1$, $v = 1$, and $s = 2/3$. The constant prefactor is thus equal to 2.357! The simulation value is 2.65. Considering that the above $\sigma_{\mathrm{a}}$ obtained by summing over $n$ is only approximate (due to the interpolation of discrete $k_i$'s to construct the continuous $k(x)$), and that there is approximation using $\log\beta$ (for $\beta$ near one), this is a quite remarkable agreement.

## 5. Concluding remarks

Based on earlier works on propagation of shocks in a periodic medium and propagation of shocks in noisy Burgers equations, we postulate that a shock will propagate in a nonlinear random medium with a mean speed given by a Rankine–Hugoniot-type relation, and its location (properly centered and normalized) tends to a Gaussian random variable for large times. The numerical scheme used to simulate the large time propagation of the shock in the moving frame has been extensively tested for different standard deviations and correlation lengths of the Langmuir coefficient. The computed mean shock position remains close to the postulated value, and the standard deviation of shock position increases linearly with $\sqrt{t}$, which corroborates the Gaussian hypothesis. Furthermore, at a given time, the statistical tests performed do not allow to reject this hypothesis. On top of the Gaussian behavior for which the theory provides ample insight, an empirical relation $\sigma_x = c\sigma_k\sqrt{l_c t}$ between the standard deviation of the shock position and the characteristics of the random medium is numerically illustrated.

We also found an analytical expression for the front standard deviation which agrees with the numerically discovered empirical front standard deviation formula when restricted to the simulation parameters. The rigorous mathematical justification of these findings is an open problem for the future. The two-time statistics of the shock position, namely its correlation length, is also an interesting problem which remains to be investigated. We believe that our present results will guide the analysis of field data in that if the random medium has a finite correlation length then one gets Gaussian statistics for front fluctuations (with an explicit formula for front statistics), while if the correlation length is infinite then one may well encounter anomolous scalings and non-Gaussian front statistics.

## Acknowledgements

The work of M.P. was done during her visit at Institut für Angewandte Mathematik, Universität Heidelberg, Germany. The work of J.X. was partially supported by NSF grants DMS-9302830, and DMS-9625680.

## References

[1] P. Billingsley, *Convergence of Probability Measures* (Wiley, New York, 1968).
[2] W.J.P. Bosma and S.E.A.T.M. van der Zee, Transport of reacting solute in a one-dimensional chemically heterogeneous porous medium, Water Resources Research 29(1) (1993) 117–131.
[3] W.J.P. Bosma, S.E.A.T.M. van der Zee and C.J. van Duijn, Plume development of a nonlinearly adsorbing solute in heterogeneous porous formations, Water Resources Research 32 (1996) 1569–1584.
[4] L. Breiman, *Statistics with a View toward Applications* (Houghton Mifflin Company, 1973).
[5] C. Dawson, C.J. van Duijn and R. Grundy, Large time asymptotics in contaminant transport in porous media, SIAM J. Appl. Math. 56(4) (1996) 965–993.

[6] R.E. Grundy, C.J. van Duijn and C.N. Dawson, Asymptotic profiles with finite mass in one-dimensional contaminant transport through porous media: Fast reaction case, Quart. J. Mech. Appl. Math. 47 (1994) 69–106.
[7] A.M. Il'in and O.A. Oleinik, Behavior of the solutions of the Cauchy problem for certain quasilinear equations for unbounded increase of time, Amer. Math. Soc. Transl. Ser. 2 42 (1964) 19–23.
[8] P.D. Lax, Hyperbolic systems of conservation laws and the mathematical theory of shock waves, Philadelphia SIAM Regional Conf. Ser. in Appl. Math. 11 (1973).
[9] S. Osher and J. Ralston, $L_1$-stability of travelling waves with applications to convective porous media flow, Comm. Pure. Appl. Math. 35 (1982) 737–749.
[10] S.E.A.T.M. van der Zee and W.H. van Riemsdijk, Transport of reactive solute in spatially variable soil systems, Water Resources Research 23(11) (1987) 2059–2069.
[11] C.J. van Duijn and P. Knabner, Solute transport in porous media with equilibrium and nonequilibrium multiple sites adsorption, travelling waves, J. Reine Angew. Math. 415 (1991) 1–49.
[12] C.J. van Duijn and P. Knabner, Travelling waves in the transport of reactive solutes through porous media, adsorption and binary ion exchange: Parts I and II, Transport in Porous Media 8 (1992) 167–194 and 199–225.
[13] J. Wehr and J. Xin, White noise perturbation of the viscous shock fronts of the Burgers equation, Comm. Math. Phys. (1996) 183–203.
[14] J. Wehr and J. Xin, Front speed in a Burgers equation with random flux, J. Statist. Phys. 88(3/4) (1997) 843–871.
[15] J.X. Xin, Existence of multidimensional traveling waves in transport of reactive solutes through periodic porous media, Arch. Rat. Mech. Anal. 128(1) (1994) 75–103.
[16] J.X. Xin, Stability of traveling waves of a solute transport equation, J. Differential Equations 135(2) (1997) 269–298.